Enhanced electrochemical performance of SrF$_2$-modified Li$_4$Ti$_5$O$_{12}$ composite anode materials for lithium-ion batteries

CrossMark

Xing Li [a],[*], Xing Zhao [a], Peng-xiao Huang [a], Ming-shan Wang [a], Yun Huang [a], Ying Zhou [a], Yuan-hua Lin [a], Mei-zhen Qu [b], Zuo-long Yu [b]

[a] The Center of New Energy Materials and Technology, School of Materials Science and Engineering, Southwest Petroleum University, Chengdu 610500, China
[b] Chengdu Institute of Organic Chemistry, Chinese Academy of Science, Chengdu 610041, China

ARTICLE INFO

ABSTRACT

The commercial Li$_4$Ti$_5$O$_{12}$ (LTO) is successfully modified by SrF$_2$ via a low temperature coprecipitation process. The results indicate that Sr^{2+} and F$^-$ do not co-dope into the bulk phase of the LTO, but instead form a SrF$_2$ coating layer on the surface of the LTO. The suitable SrF$_2$ buffer layer could cover the catalytic active sites of the LTO and suppress the electrolyte reduction decomposition on the surface of the LTO, which means that the SrF$_2$ modification is favorable to suppress gas generation of the LIBs using LTO as anode material during charge/discharge cycles and storage. Moreover, according to optimized the amount of SrF$_2$, the 2 wt% of SrF$_2$ in the SrF$_2$ modified LTO composites exhibits the best rate capability and an excellent cyclic performance.

© 2016 Elsevier B.V. All rights reserved.

1. Introduction

Ti-based anodes materials such as Li$_4$Ti$_5$O$_{12}$ (LTO) and TiO$_2$ [1,2] have been regarded as promising materials for Lithium ion batteries. Especially, the LTO has been regarded as an alternative to graphite anode material for long life type lithium-ion power batteries because of its negligible volume change during charge and discharge, high safety, thermal stability, and long cycle life within a wide operating temperature range [3]. Unfortunately, the low electronic conductivity and the sluggish lithium ion diffusion in LTO make it suffer from poor high-rate charge/discharge capabilities [4]. Many approaches, including carbon coating [5,6], metal and nonmetal ion doping [7–9], developing nano-sized particles [10–12] or porous particles [13] and forming composites with CNTs [14,15], Graphene [16–18], metals or metal oxides [19–21], have been pursued to improve the power performance of LTO.

Even after a variety of efforts based on the above strategies, the LTO anode is still not considered as the most preferable choice for large-scale applications by the power lithium ion batteries (LIBs) industries. This is mainly due to the LIBs using LTO as anode material existing severe gassing during charge/discharge cycles and storage, especially at elevated temperatures [22,23]. To date, there are only a few reports that specifically refer to the gassing behavior of LTO electrodes [22–26]. Recently, the reason for the gassing behavior of the LTO anode has been revealed, which was confirmed originating from interfacial reactions between LTO and surrounding alkyl carbonate solvents [27]. Carbon coating on the surface of the LTO was reported as an effectively approach to suppress the gas generation of the LTO anode, which was mainly due to the carbon layer could cover the catalytic active sites of the LTO and separate the LTO from the electrolyte [28]. Furthermore, the carbon coating was favorable to form a successive solid electrolyte interface (SEI) film on the surface of the LTO anode, which could prevent the further reduction decomposition of the electrolyte [28]. However, the existence of carbon coating is likely to be a threat to the safety of LTO anode batteries [29]. Therefore, a zero carbon content and safe coating layer should be proposed during the modified process of the LTO.

Surface modification [30–32], especially with fluoride has been proved to be an effective way to enhance the cyclic stability of the layered oxides of the cathodes [33–40]. The improved

---

* Corresponding author. Southwest Petroleum University, Xindu Road 8, Chengdu 610500, China.
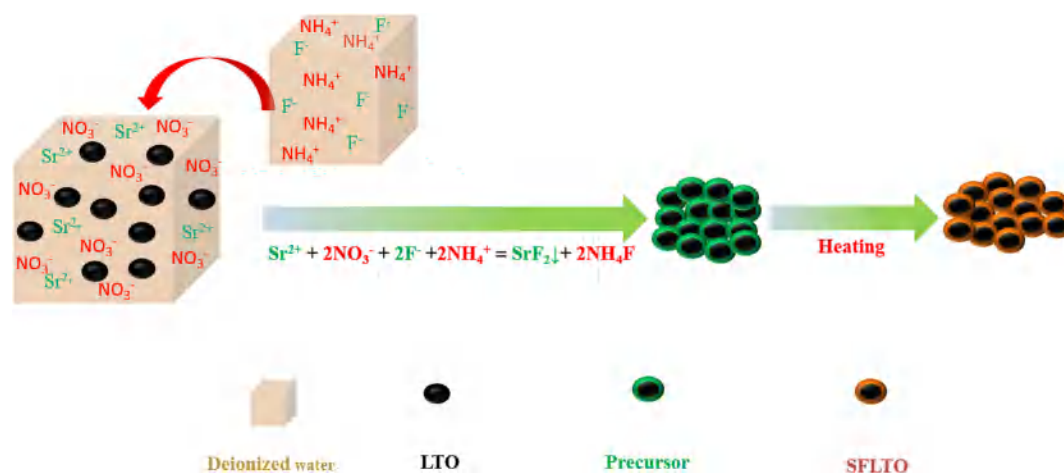E-mail address: lixing@swpu.edu.cn (X. Li).

Fig. 1. Schematic diagram of the synthesis of mSFLTO (m = 0.5, 1.0, 2.0, 3.0) samples by using a coprecipitation method.

electrochemical performance was tentatively attributed to the buffer layer provided by the fluoride coating, which could reduce the activity of the extracted of oxygen and suppress the electrolyte decomposition on the surface of the cathode material [35]. The AlF$_3$ [34,36], LiF [38], SrF$_2$ [39], and CaF$_2$ [40] have been successfully coated on the surface of the cathode materials and the enhanced electrochemical performances of the cathodes have been achieved. Given this association, the fluoride buffer layer might also can cover the catalytic active sites of the LTO and suppress the electrolyte reduction decomposition on the surface of the LTO anode. In our previous work [29], we have reported an AlF$_3$ modified LTO composite via a low temperature preparation process. We found that only part of the Al^{3+} and F$^-$ were co-doped into the bulk phase of the LTO particles, while the rest of the Al^{3+} and F$^-$ remained on the surface of the LTO particles forming a thin AlF$_3$ coating layer. The results indicated that AlF$_3$ modified LTO anode could obviously suppress the electrolyte reduction decomposition, and we believed that should be ascribed to the AlF$_3$ buffer layer could cover the catalytic active sites of the LTO and separate it from the electrolyte. Among the fluoride, the SrF$_2$ has better stability than others in the electrolyte [39], which should be a more preferable fluoride coating material for the LTO anode. In the present study, we report a facile method to make SrF$_2$ modified LTO composite via a low-temperature reaction. The SrF$_2$ modified LTO composites are characterized and their enhanced rate capability and cycling stability are discussed. In addition, the interfacial reactions between SrF$_2$ modified LTO composites and electrolyte are also investigated.

2. Experimental

2.1. Materials synthesis

The SrF$_2$ modified LTO samples were prepared following the procedures described in literature for SrF$_2$ modified cathode material.[47] Commercial LTO (Chengdu Xingneng New Materials Co., LTD) powder was used for this study. Ammonium fluoride (NH$_4$F, 98%, Sigma-Aldrich) and strontium nitrate (Sr(NO$_3$)$_2$, 98%, Sigma-Aldrich) were added at a fixed stoichiometric molar ratio of Sr^{2+}:F$^-$ = 1:2 and at different amounts. After being constantly stirred at 80 °C for 5 h, filtrated and purified, the mixed solid powders were calcined at 400 °C for 5 h under argon atmosphere. The obtained SrF$_2$-modified LTO samples are denoted mSFLTO (m = 0.5, 1.0, 2.0, 3.0), where m is the weight percentage of SrF$_2$ in

the composites of SrF$_2$ modified LTO samples.

2.2. Materials characterization

Powder X-ray diffraction (XRD, Xpert MPD DY1219) with Cu K$_\alpha$ radiation was used to identify the crystal lattice parameters of the commercial LTO and the mSFLTO samples. Microstructure and morphology of the prepared samples were observed via scanning electron microscope (SEM, FEI INSPECT-F) with an energy-dispersive detector (EDS) and transmission electron microscope (TEM, Libra200FE). The chemical composition of the mSFLTO sample was determined by X-ray photoelectron spectroscopy (XPS, PHI5600 Physical Electronics).

2.3. Coin-type half cells electrochemical measurements

The working electrode was prepared by coating the mixed slurries (85 wt% mSFLTO composites or pristine LTO, 10 wt% conductive Super-P and 5 wt% LA-132 binder) onto an alumina foil using a doctor blade, with a 100 μm gap. The weight of active material in the working electrode was 3.50 mg, and the geometrical area of the working electrode was 1.54 cm^2. The working electrode was then dried in a vacuum oven at 80 °C for 12 h to remove any residual solvent and possible adsorbed moisture. Electrochemical measurements were performed using coin-type half cells assembled in an argon-filled glove box. The cathode of the coin-type half cell was the as-prepared working electrode, the counter and reference electrode was lithium metal, the separator was Celgard 2400, and the electrolyte was 1 M LiPF$_6$/EC:DEC:DMC (1:1:1 in volume). Galvanostatic charge and discharge experiments were carried out on BTS-5V20 mA cell test instruments (NEWARE Electronic Co. Ltd) between cut-off voltages of 1–3 V at different charge/discharge rates at 25 °C. Cyclic voltammograms (CV) were recorded from 1 V to 3 V with a scan rate of 0.2 mV/s by using the Auto-lab Pgstat302N electrochemical workstation. The electrochemical impedance spectrum (EIS) was measured by using a Solatron 1260 Impedance Analyzer in the frequency range 10^{-2}–10^5 Hz with a potential perturbation at 10 mV. The coin-type half cells that used for the EIS measurements were at half state of charge.

In order to investigate the interfacial reactions between the working electrode and the electrolyte, the coin-type half cells after the galvanostatic charge and discharge tests were transferred to an argon-filled glove box and then disassembled. The working
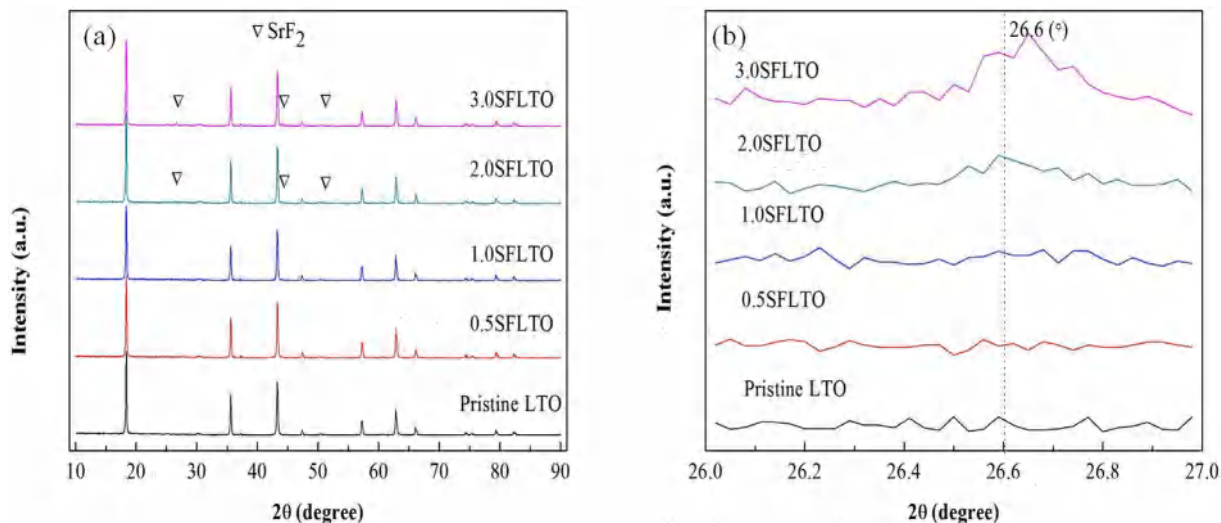
Fig. 2. XRD patterns (a) and enlarged peaks at $2\theta = 26.0°-27.0°$ (b) of commercial LTO and mSFLTO (m = 0.5, 1.0, 2.0, 3.0) composites.
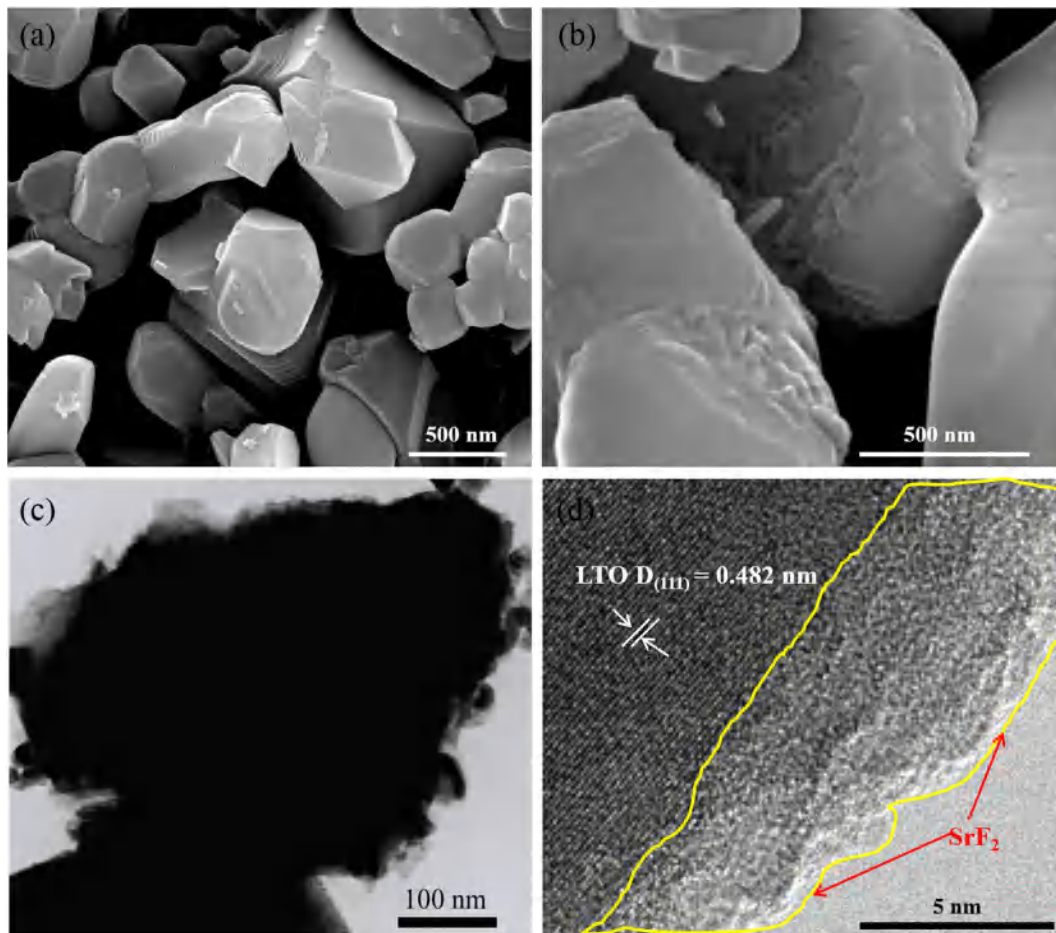

Fig. 3. SEM images of commercial LTO (a), 2.0SFLTO (b) and TEM images of 2.0SFLTO (c, d).

electrodes were rinsed using dimethyl carbonate (DMC) to remove the electrolyte from the electrode surface and then drying in the glove box to remove the residual DMC. The surface morphology of the working electrodes was examined with a field emission scanning electron microscopy (SEM, FEI INSPECT-F).

3. Results and discussion

Fig. 1 shows a schematic diagram of the synthesis of mSFLTO (m = 0.5, 1.0, 2.0, 3.0) samples by using a coprecipitation method. Firstly, an amount of Sr(NO$_3$)$_2$ and NH$_4$F was dissolved in deionized
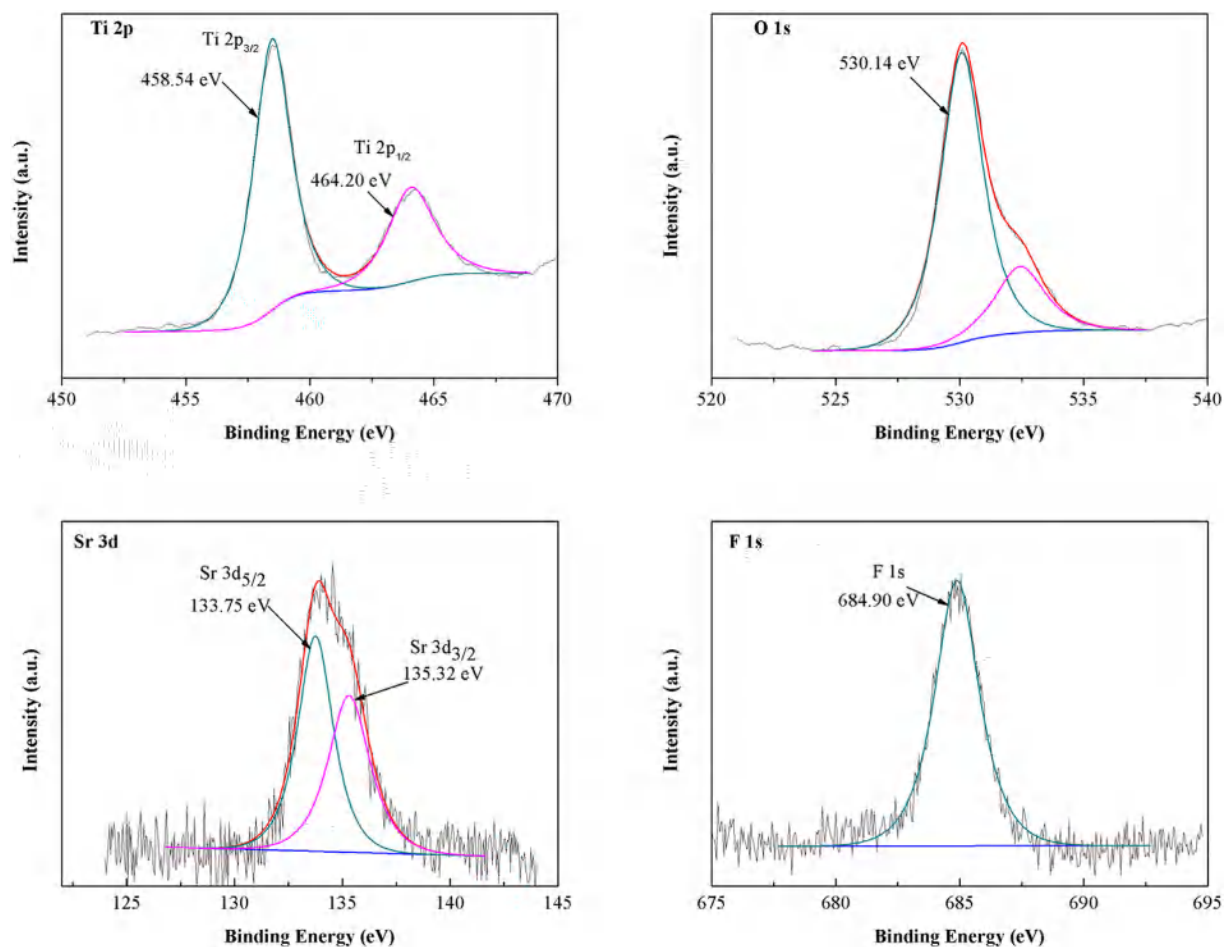
Fig. 4. XPS spectrum of 2.0SFLTO, Sr 3d and F 1s spectrum.

water to form a stable solution, respectively. Then the commercial LTO powder was added to the $Sr(NO_3)_2$ solution with sufficient sonication to form an uniform suspension. Finally, the stoichiometric molar ratio of NH_4F solution ($Sr^{2+}:F^- = 1:2$) was added to the above suspension with a speed of 1–2 ml/min under vigorous stirring. While the F^- meeting the Sr^{2+}, as the solubility product constant (K_{sp}) value for the SrF_2 is very small (2.5×10^{-9}), therefore, the SrF_2 precipitation would form and adhere to the surface of the LTO particles. After filtration and purification, the above mentioned precursor was then heated at 400 °C for 5 h under argon atmosphere to obtain the mSFLTO samples.

Fig. 2a shows the XRD patterns of the mSFLTO (m = 0.5, 1.0, 2.0, 3.0) and the commercial LTO. All the five samples show the major peaks of cubic LTO (JCPDS No. 49-0207), which indicate that SrF_2-modified process do not obviously change the crystal structure of the LTO during heat treatment. From Fig. 2a, it can also be observed the extra peaks for SrF_2 (JCPDS No. 06-0262) marked with del ($\triangledown$) in the composites of 2.0SFLTO and 3.0SFLTO. The peaks of the SrF_2 in the composites of 0.5SFLTO and 1.0SFLTO are not observed should attribute to the low weight percentage in the composites. For a clear observation, the major peak for the SrF_2 ($2\theta = 26.6°$) is magnified in Fig. 1b.

The SEM of SrF_2-modified LTO are shown in Fig. 3, it can be observed that the commercial LTO (Fig. 3a) shows a well-crystallized structure and smooth surface, however, it can also be obviously observed that there is a coating layer on the surface of the composite of 2.0SFLTO (Fig. 3b). Furthermore, the existing of the

coating layer on the surface of the 2.0SFLTO composite can be further identified via the TEM images (Fig. 3c, d). Fig. 4 shows the XPS measurement of the 2.0SFLTO. The binding energy for the Ti $2p_{3/2}$ and $2p_{1/2}$ is 458.54 eV and 464.20 eV, which should be related to the Ti^{4+} in the LTO [41]. The O 1s spectrum has a binding value of 530.14 eV, which should be the oxygen predominantly bonded to Ti ions [42]. An additional low-intensity peak can be observed in the O 1s spectrum, which might be due to the adsorbed water or surface OH^- groups [43]. The Sr $3d_{5/2}$ and $3d_{3/2}$ peaks at 133.75 eV and 135.32 eV are related to Sr^{2+}, while the F 1s peak at 684.90 eV is related to F^- [44]. This indicates that the coating layer on the surface of the 2.0SFLTO composite contains Sr^{2+} and F^-. Combining the results of the XRD, SEM and TEM of the sample, it can deduce that the coating layer on the surface of the LTO should be mainly SrF_2. Fig. 5 exhibits the distributions of the element O, Ti, Sr and F in the tested area (SEM image in Fig. 5), respectively. It can be observed from Fig. 5 that all the elements have homogeneous distributions, which indicates that the SrF_2 buffer layer is uniformly covered on the surface of the LTO.

Fig. 6 shows the SEM images of the LTO and 2.0SFLTO electrodes after rate tests (0.5 C, 10 cycles; 1.0 C, 10 cycles; 3.0 C, 10 cycles; 5.0 C, 10 cycles; 10.0 C, 10 cycles; 20.0 C, 10 cycles at the cut-off voltages of 1–3 V). As shown in Fig. 6a, it can be observed there is some black matter (which has been regarded as SEI film by He et al. [27,28]) formed on the surface of the commercial LTO electrode at the cut-off voltages of 1–3 V. The reason for the formed SEI film could be ascribed to the interfacial reactions between the LTO
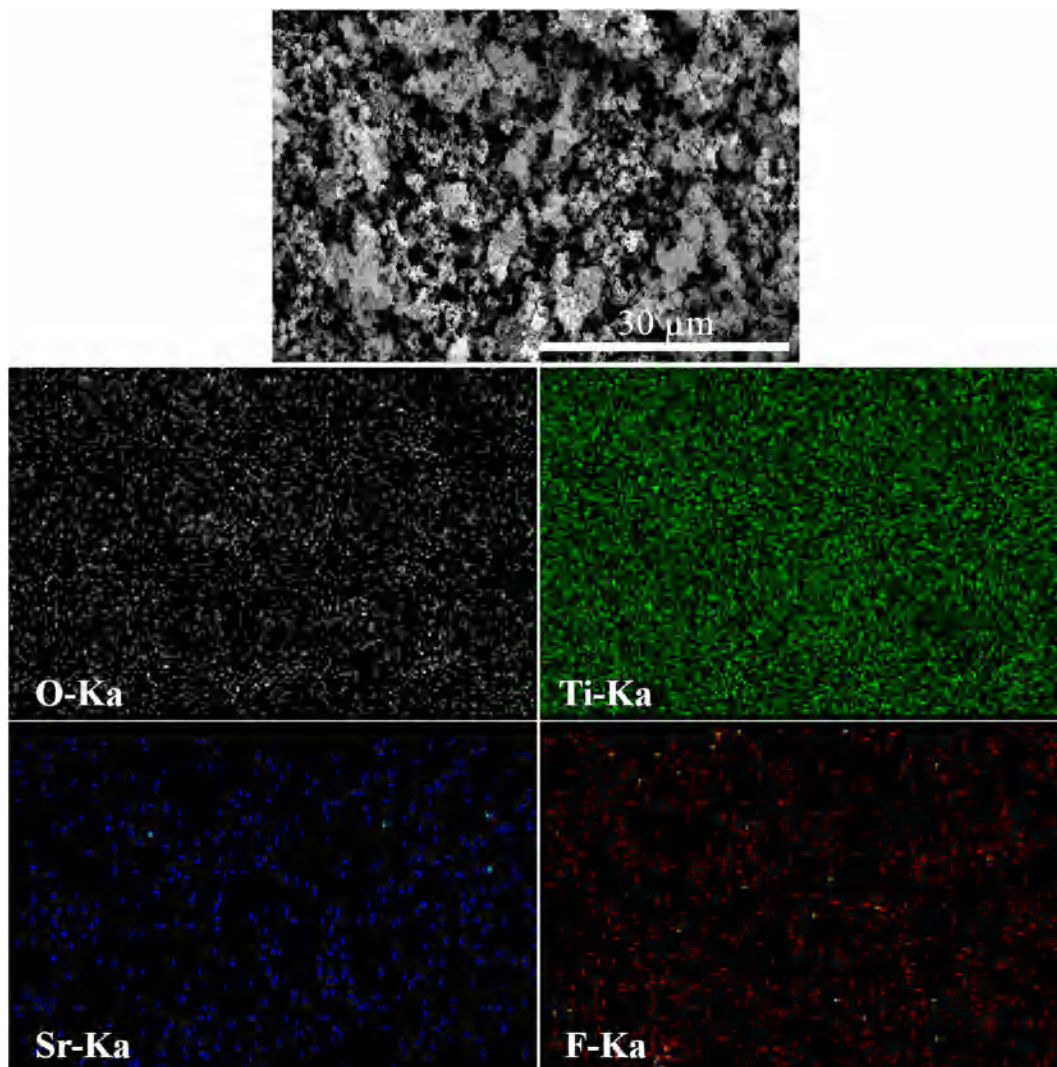
Fig. 5. EDS elemental mapping (O, Ti, Sr and F) for the selected area of 2.0SFLTO. The SEM image (top) shows the selected area corresponding to the elemental mapping of the 2.0SFLTO.
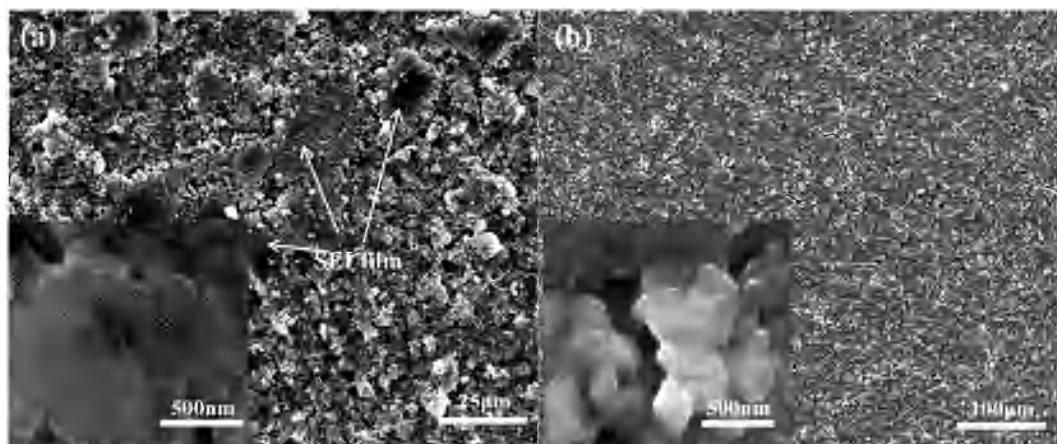
Fig. 6. SEM images of the commercial LTO (a) and 2.0SFLTO (b) electrodes after galvanostatic discharge and charge tests at the cut-off voltages of 1–3 V.

and the surrounding alkyl carbonate solvents [27]. The interfacial side reactions can lead to severe gassing during charge/discharge cycles and storage. Furthermore, the electrode polarization of the LTO will increase and its discharge specific capacity also will become poor. However, as shown in Fig. 6b, it can be observed that there is almost no SEI film formed on the surface of the 2.0SFLTO
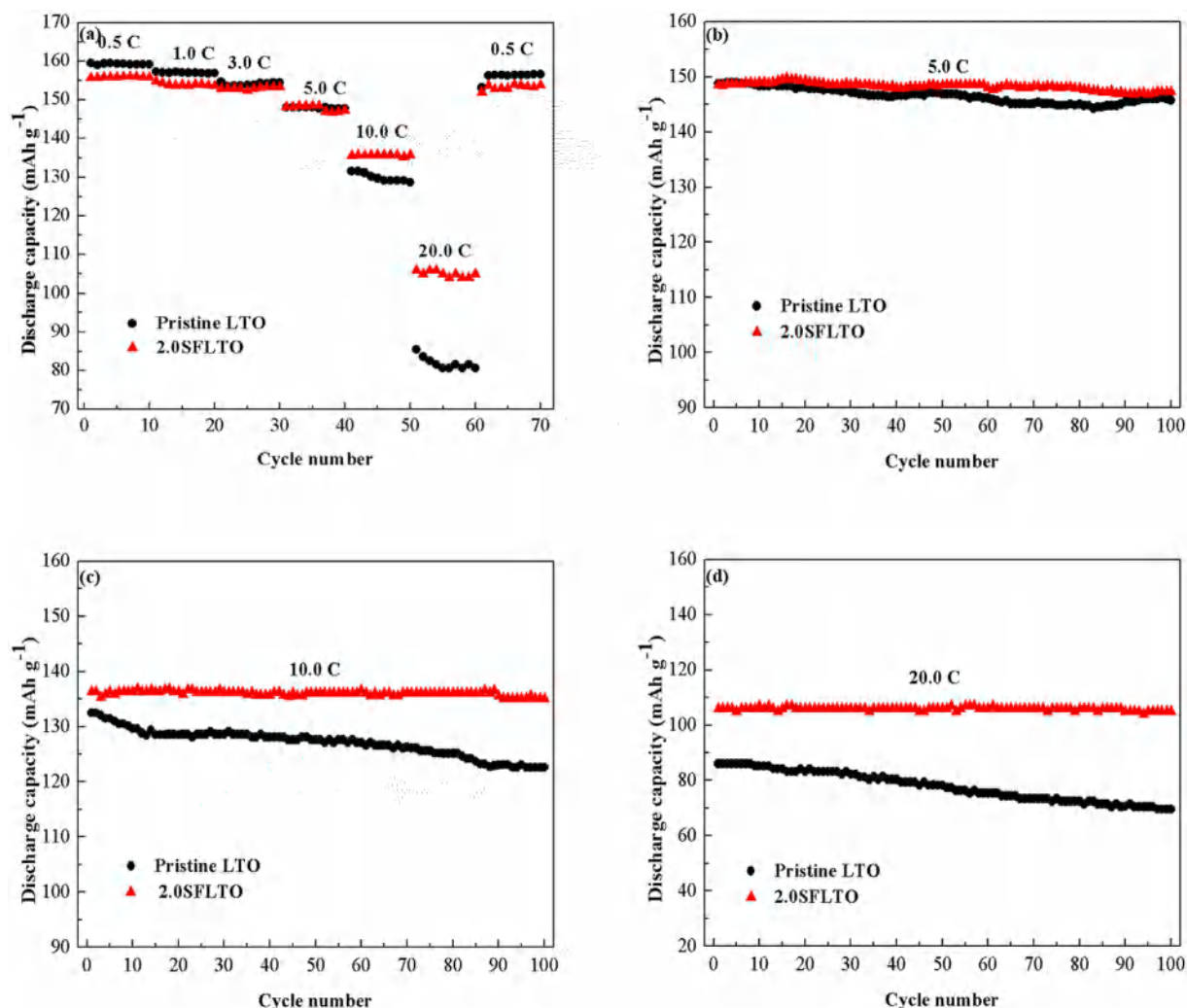
Fig. 7. Rate capability (a) and cyclic performances (b) of the pristine (commercial). LTO and 2.0SFLTO at the cut-off voltages of 1–3 V.

electrode at the cut-off voltages of 1–3 V. This indicates that the SrF$_2$ coating layer can suppress the interfacial reactions between the electrode and the electrolyte by covering the catalytic active sites of the LTO.

Fig. 7a shows the rate capability of the pristine (commercial) LTO and 2.0SFLTO at different rates from 0.5 C, 1.0 C, 3.0 C, 5.0 C, 10.0 C–20.0 C and then in returned from 20.0 C to 0.5 C at the cut-off voltages of 1–3 V. The charge–discharge processes of the samples were carried out for 10 cycles at 0.5 C, 1.0 C, 3.0 C, 5.0 C, 10.0 C, 20.0 C and again at 0.5 C, respectively. It can be observed that discharge specific capacity of the commercial LTO is 159 mA h/g, 157 mA h/g and 154 mA h/g at the rates of 0.5 C, 1.0 C and 3.0 C, and the discharge specific capacity of the 2.0SFLTO is 157 mA h/g, 154 mA h/g and 153 mA h/g at the same rates mentioned above. This indicates that the 2.0SFLTO shows slightly lower discharge specific capacity than the commercial LTO at the low rates, which should be ascribed to that the SrF$_2$ buffer layer is an electrochemical inert material and giving no contribution to the charge/discharge specific capacity [39]. However, as show in Fig. 7a, it can also be observed that the 2.0SFLTO exhibits obviously higher discharge specific capacity than that of the commercial LTO at the high rates of 5.0 C, 10.0 C and 20.0 C. The discharge specific capacity of the 2.0SFLTO is 149 mA h/g, 136 mA h/g and 107 mA h/g at the rates of 5.0 C, 10.0 C and 20.0 C, while the discharge specific capacity of the

commercial LTO is only 140 mA h/g, 129 mA h/g and 82 mA h/g at the same high rates. This should be attributed to that there is more SEI film formed on the surface of the commercial LTO electrode than that of the 2.0SFLTO electrode (as shown in the SEM images of Fig. 6a and b) during the high rates charge/discharge processes. The SEI film comes from the interfacial reactions between the LTO and the surrounding alkyl carbonate solvents especially at high rates (heavy current) charge/discharge processes [27], which could lead to the electrode polarization and results in poor discharge specific capacity. For the 2.0SFLTO electrode, as the SrF$_2$ buffer layer could cover the catalytic active sites of the LTO and separate it from the electrolyte, therefore there is almost no SEI film formed on the surface of the 2.0SFLTO electrode during the charge/discharge process (as shown in the SEM images of Fig. 6b). However, for the commercial LTO electrode, as the interfacial reactions between the LTO and the surrounding alkyl carbonate solvents especially at high rates, there has formed a thick SEI film on the electrode (as shown in the SEM images of Fig. 6a), which makes the commercial LTO exhibits higher electrode polarization and lower discharge specific capacity than that of the 2.0SFLTO at the high rates of 5.0 C, 10.0 C and 20.0 C.

Fig. 7b compares the cyclic performances of the pristine (commercial) LTO and 2.0SFLTO at the rate of 5.0 C. As shown in Fig. 7b, at 5.0 C, the first discharge specific capacity, the 100th discharge
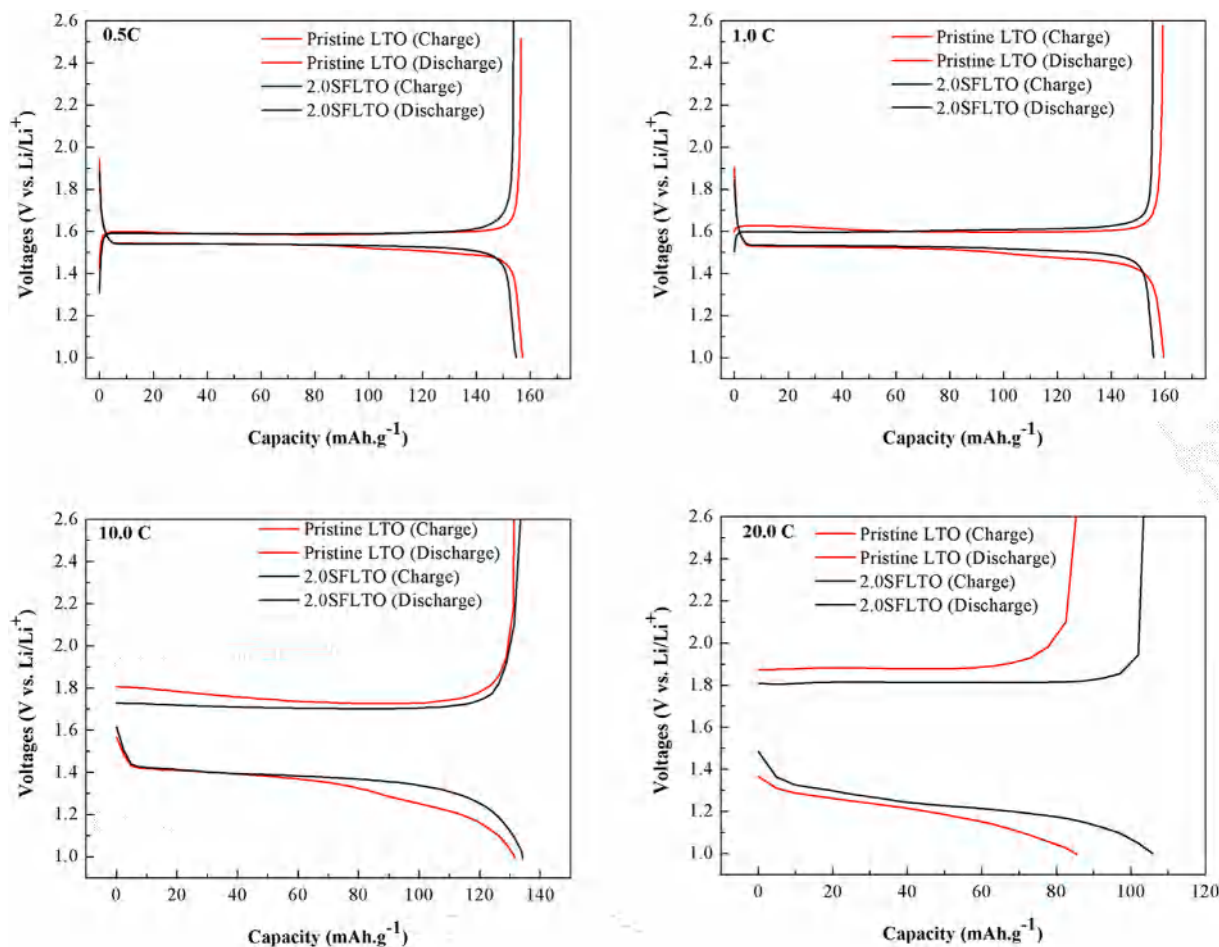
Fig. 8. Charge and discharge curves of the pristine (commercial) LTO and 2.0SFLTO electrodes at the rates of 0.5 C, 1.0 C, 10.0 C and 20.0 C.

specific capacity and the capacity retention ratio of the 2.0SFLTO are 148 mA h/g, 147 mA h/g and 99.3%, respectively, while these values for the pristine LTO are 140 mA h/g, 137 mA h/g and 97.9%, respectively. Moreover, Fig. 7c and d further compare the cyclic performances of the pristine (commercial) LTO and 2.0SFLTO at the rate of 10.0 C and 20.0 C. As shown in Fig. 7c, at 10.0 C, the first discharge specific capacity, the 100th discharge specific capacity and the capacity retention ratio of the 2.0SFLTO are 136 mA h/g, 135 mA h/g and 99.3%, respectively, while these values for the pristine LTO are only 132 mA h/g, 122 mA h/g and 92.6%, respectively. As shown in Fig. 7d, at 20.0 C, the first discharge specific capacity, the 100th discharge specific capacity and the capacity retention ratio of the 2.0SFLTO are 106 mA h/g, 105 mA h/g and 99.1%, respectively, while these values for the pristine LTO are only 86 mA h/g, 70 mA h/g and 81.4%, respectively. These results indicate that the 2.0SFLTO exhibits better cyclic performances than that of the pristine LTO at the high rate of 5.0 C. 10.0 C and 20.0 C.

Fig. 8 shows the charge and discharge curves of the commercial LTO and 2.0SFLTO electrodes at the low rates of 0.5 C, 1.0 C and the high rates of 10.0 C, 20.0 C, respectively. As known, the margins between the charge and discharge plateau potentials could be corresponding to the polarization of the electrode [14]. As shown in Fig. 8, it can be observed that the margins between the charge and discharge plateau potentials of the 2.0SFLTO are slightly larger than that of the commercial LTO at the low rates of 0.5 C and 1.0 C. This indicates that the electrode resistance of the 2.0SFLTO is slightly larger than that of the commercial LTO at the low rates, which

should be ascribed to the insulated coating layer of the SrF_2. However, from Fig. 8, it can be observed that the margins between the charge and discharge plateau potentials of the 2.0SFLTO are obviously smaller than that of the commercial LTO at the high rates of 10.0 C and 20.0 C. This indicates that the electrode resistance of the 2.0SFLTO is much smaller than that of the commercial LTO at the high rates. For the commercial LTO electrode, as the existing of interfacial reactions between the LTO and the surrounding alkyl carbonate solvents, therefore there is more SEI film formed on the surface of the electrode especially at high rates (such as 10.0 C and 20.0 C) and which results in it has larger electrode polarization than the 2.0SFLTO.

Fig. 9a shows the electrochemical impedance spectrum (EIS) of the pristine LTO and the 2.0SFLTO electrodes (fresh electrodes) which did not experienced the galvanostatic discharge and charge tests at the cut-off voltages of 1–3 V. Fig. 9b shows the electrochemical impedance spectrum (EIS) of the pristine LTO and the 2.0SFLTO electrodes which have experienced the galvanostatic discharge and charge tests at different rates (0.5 C, 10 cycles; 1.0 C, 10 cycles; 3.0 C, 10 cycles; 5.0 C, 10 cycles; 10.0 C, 10 cycles; 20.0 C, 10 cycles) at the cut-off voltages of 1–3 V. All of the above electrodes are at a charge state of 1.55 V while executing the EIS tests. The solid lines are fitted by the equivalent circuit as inserted in Fig. 8a and b. The R_e and $R_{(sf+ct)}$ ($R_{sf} + R_{ct}$) in the equivalent circuit represent the electrolyte resistance and cell components, surface film resistance and the charge transfer resistance, respectively [45]. The R_b represents the electronic resistivity of the active material
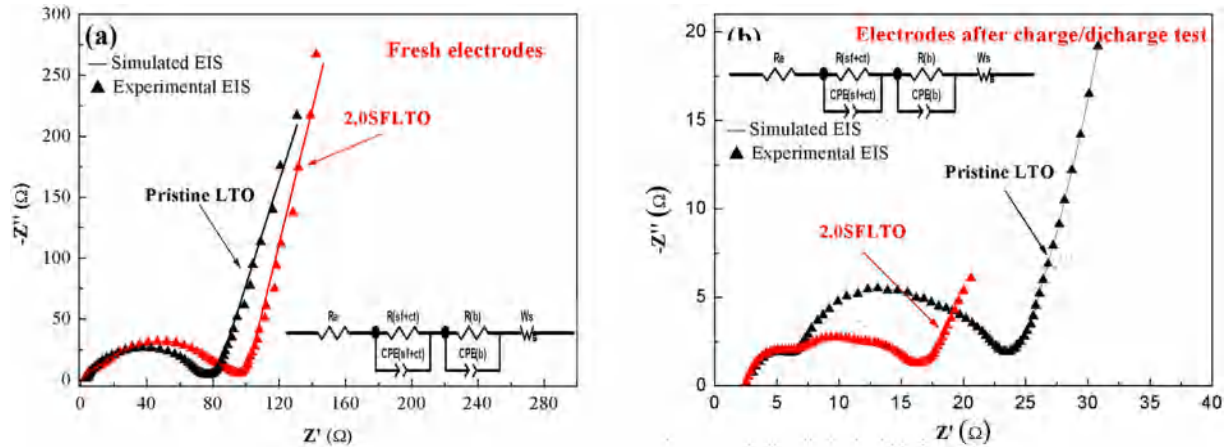
Fig. 9. Electrochemical impedance spectrums of the fresh electrodes of pristine (commercial) LTO and 2.0SFLTO (a), and electrochemical impedance spectrums of the pristine (commercial) LTO and 2.0SFLTO electrodes that have experienced the galvanostatic discharge and charge tests (b).

Table 1
Fitted parameters of equivalent circuit of Fig. 9a and b.

Samples	Fresh electrodes				After galvanostatic charge and discharge tests			
	$R_e(\Omega)$	$R_{sf+ct}(\Omega)$	$R_b(\Omega)$	CPE_{sf+ct} (μF)	$R_e(\Omega)$	$R_{sf+ct}(\Omega)$	R_b (Ω)	CPE_{sf+ct} (μF)
LTO	2.3	3.4	68.6	18.5	2.9	14.6	7.8	44.9
2.0SFLTO	2.5	4.3	76.9	32.6	2.6	8.8	5.4	36.7
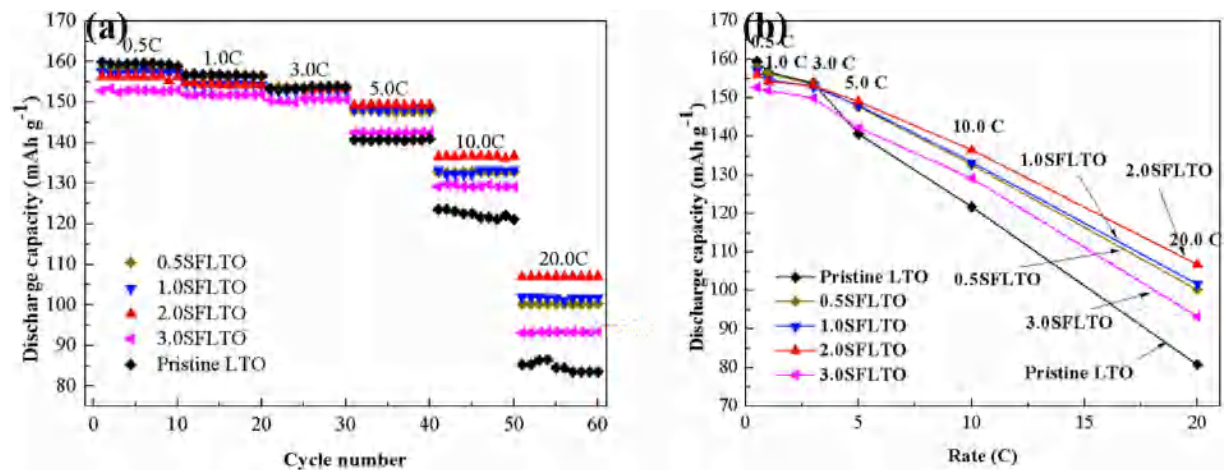
Fig. 10. Rate capability of the pristine LTO and the mSFLTO (m = 0.5, 1.0, 2.0, 3.0) composites (a) and the discharge specific capacity of the pristine LTO and the mSFLTO (m = 0.5, 1.0, 2.0, 3.0) composites as a function of the charge/discharge rates (b).

and the ionic conductivity in the pores of the electrode [46]. The CPE represent the surface film and double layer capacitance. The W_s is the Warburg resistance associated with the solid state diffusion of Li-ion through the LTO lattice. The Nyquist plots for both the pristine LTO and the 2.0SFLTO consist of two depressed semicircles in the high to medium frequency range and an infinite diffusion line in the low frequency range. The fitted data from the equivalent circuit is listed in Table 1. For the fresh electrodes that did not experienced the galvanostatic discharge and charge tests, there it can be observed that the $R_{(sf+ct)}$ and R_b values of the 2.0SFLTO are slightly larger than that of the pristine LTO. This indicates that the fresh electrode of the 2.0SFLTO has larger electrode polarization than that of the fresh electrode of the pristine LTO, which should be ascribed to the insulated coating layer of the SrF$_2$. However, for the electrodes that have experienced the galvanostatic discharge and

charge tests, it can be observed that the $R_{(sf+ct)}$ and R_b values of the 2.0SFLTO are obviously smaller than that of the pristine LTO. This indicates that the pristine LTO has larger electrode polarization than the 2.0SFLTO after galvanostatic discharge and charge tests, which should be attributed to the more amount of SEI film formed on the surface of the pristine LTO electrode. For the 2.0SFLTO electrode, however, as the SrF$_2$ coating layer could suppress the interfacial reactions between the LTO and the electrolyte, therefore, which leads to less amount of SEI film formed on the electrode and less electrode polarization. Furthermore, as shown in Table 1, it can be observed that the $R_{(sf+ct)}$ values of the pristine LTO after galvanostatic discharge and charge tests increase to about 4 times its initial (fresh). This further indicates that there has been more SEI film formed on the electrode during the galvanostatic discharge and charge tests. However, there is obviously less increment of

the $R_{(sf+ct)}$ values for the 2.0SFLTO electrode after galvanostatic discharge and charge tests while comparing with its fresh electrode, which indicates that there has been less SEI film formed on the electrode during the galvanostatic discharge and charge tests.

The SrF_2 buffer layer is an electrochemical inert and insulated material, which could cover the catalytic active sites of the LTO and suppress the electrolyte reduction decomposition on the surface of the SrF_2 modified LTO electrode. However, as the SrF_2 buffer layer gives no contribution to the charge/discharge specific capacity and can increase the electrode resistance, therefore there should be an appropriate amount of SrF_2 in the composite of mSFLTO. Fig. 10a shows the rate capability of pristine LTO and the mSFLTO (m = 0.5, 1.0, 2.0, 3.0) composites. Fig. 10b shows the discharge specific capacity of the pristine (commercial) LTO and the mSFLTO (m = 0.5, 1.0, 2.0, 3.0) as a function of the charge/discharge rate. As shown in Fig. 10a and b, it can be observed that all the mSFLTO (m = 0.5, 1.0, 2.0, 3.0) exhibit a slightly lower discharge specific capacity than that of the pristine (commercial) LTO at low rates of 0.5 C, 1.0 C and 3.0 C. Furthermore, it can be observed that the discharge specific capability of the mSFLTO (m = 0.5, 1.0, 2.0, 3.0) at low rates (0.5 C, 1.0 C, 3.0 C) decreases with the increase of the weight percentage of SrF_2 in the mSFLTO composites. These should be ascribed to the electrochemical inert SrF_2 giving no contribution to the charge/discharge specific capacity. However, while at high rates of 5.0 C, 10.0 C and 20.0 C, it can be observed that all the mSFLTO (m = 0.5, 1.0, 2.0, 3.0) show higher discharge capacity than the pristine (commercial) LTO, and the 2.0SFLTO exhibits the highest discharge capacity among them. This should be attributed to that the 2 wt% of SrF_2 in the mSFLTO composite could not only well cover the catalytic active sites of the LTO but also lead to an appropriate/acceptable electrode resistance.

4. Conclusion

The SrF_2 modified LTO composites were prepared via a low-temperature reaction between LTO and SrF_2. The results showed that there was no Sr^{2+} and F^- co-doping into the bulk phase of the LTO, and instead formed a SrF_2 coating layer on the surface of the LTO particles. The mSFLTO (m = 0.5, 1.0, 2.0, 3.0) showed slightly lower discharge specific capacity than that of the pristine LTO at low rates of 0.5 C, 1.0 C and 3.0 C, which should be ascribed to that the SrF_2 coating layer was an electrochemical inert material and giving no contribution to the charge/discharge specific capacity. However, the mSFLTO (m = 0.5, 1.0, 2.0, 3.0) showed obviously higher discharge specific capacity than that of the pristine LTO at high rates of 5.0 C, 10.0 C and 20.0 C, which should be attributed to the SrF_2 buffer layer could cover the catalytic active sites of the LTO, suppress the electrolyte reduction decomposition (SEI film formation) and result in less electrode polarization. As the SrF_2 buffer layer is an electrochemical inert and insulated material, too much amount of SrF_2 could impair the discharge specific capacity and increase electrode resistance, therefore there should be an appropriate amount of SrF_2 in the composite of mSFLTO. The electrochemical results indicated that the 2.0SFLTO showed the best rate capability, which meant that the 2.0 wt% of SrF_2 in the SrF_2 modified LTO composites is appropriate.

References

[1] T. Ohzuku, A. Ueda, N. Yamamoto, J. Electrochem. Soc. 142 (1995) 1431.
[2] M.V. Reddy, X.W.V. Teoh, T.B. Nguyen, Y.Y.M. Lim, B.V.R. Chowdari, J. Electrochem. Soc. 159 (6) (2012) A762.
[3] K. Amine, I. Belharouak, Z. Chen, T. Tran, H. Yumoto, N. Ota, S.T. Myung, Y.K. Sun, Adv. Mater 22 (2010) 3052.
[4] M. Wagemaker, E.R.H. van Eck, A.P.M. Kentgens, F.M. Mulder, J. Phys. Chem. B 113 (2009) 224.
[5] G.J. Wang, J. Gao, L.J. Fu, N.H. Zhao, Y.P. Wu, T. Takamura, J. Power Sources 174 (2007) 1109–1112.
[6] G.N. Zhu, H.J. Liu, J.H. Zhuang, C.X. Wang, Y.G. Wang, Y.Y. Xia, Energy Environ. Sci. 4 (2011) 4016–4022.
[7] D. Capsoni, M. Bini, V. Massarotti, P. Mustarelli, G. Chiodelli, C.B. Azzoni, M.C. Mozzati, L. Linati, S. Ferrari, Chem, Mater 20 (2008) 4291.
[8] J.S. Park, S.H. Baek, Y.П. Jeong, B.Y. Noh, J.H. Kim, J. Power Sources 244 (2013) 527–531.
[9] C.F. Lin, M.O. Lai, L. Lu, H.H. Zhou, Y.L. Xin, J. Power Sources 244 (2013) 272–279.
[10] A.S. Prakash, P. Manikandan, K. Ramesha, M. Sathiya, J.M. Tarascon, A.K. Shukla, Chem. Mater 22 (2010) 2857.
[11] T. Doi, Y. Iriyama, T. Abe, Z. Ogumi, Chem. Mater 17 (2005) 1580.
[12] A. Guerfi, S. Sevigny, M. Lagace, P. Hovington, K. Kinoshita, K. Zaghib, J. Power Sources 119 (2003) 88.
[13] K. Amine, I. Belharouak, Z.H. Chen, T. Tran, H. Yumoto, N. Ota, S.T. Myung, Y.K. Sun, Adv. Mater 22 (2010) 3052–3057.
[14] X. Li, M.Z. Qu, Y.J. Huai, Z.L. Yu, Electrochim. Acta 55 (2010) 2978–2982.
[15] J.J. Huang, Z.Y. Jiang, Electrochim. Acta 53 (2008) 7756–7759.
[16] Y. Ding, G.R. Li, C.W. Xiao, X.P. Gao, Electrochim. Acta 102 (2013) 282–289.
[17] A.K. Rai, J. Gim, S.W. Kang, V. Mathew, L.T. Anh, J. Kang, J.J. Song, B.J. Paul, J. Kim, Mater. Chem. Phys. 136 (2012) 1044–1051.
[18] X. Guo, H.F. Xiang, T.P. Zhou, W.H. Li, X.W. Wang, J.X. Zhou, Y. Yu, Electrochim. Acta 109 (2013) 33–38.
[19] M.M. Rahman, J.Z. Wang, M.F. Hassan, D. Wexler, H.K. Liu, Adv. Energy Mater 1 (2011) 212.
[20] K.M. Kim, K.Y. Kang, S. Kim, Y.G. Lee, Curr. Appl. Phys. 12 (2012) 1199.
[21] J. Wang, H. Zhao, Q. Yang, C. Wang, P. Lv, Q. Xia, J. Power Sources 222 (2013) 196.
[22] I. Belharouak, G.M. Koenig, T. Tan, H. Yumoto, N. Ota, K. Amine, J. Electrochem. Soc. 159 (2012) A1165.
[23] K. Wu, J. Yang, Y. Zhang, C.Y. Wang, D.Y. Wang, J. Appl. Electrochem. 42 (2012) 989.
[24] A. Du Pasquier, I. Plitz, S. Menocal, G. Amatucci, J. Power Sources 115 (2003) 171.
[25] X. Lu, L. Zhao, X.Q. He, R.J. Xiao, L. Gu, Y.S. Hu, H. Li, Z.X. Wang, X.F. Duan, L.Q. Chen, J. Maier, Y. Ikuhara, Adv. Mater. 24 (2012) 3233.
[26] Z.J. Ding, L. Zhao, L.M. Suo, Y. Jiao, S. Meng, Y.S. Hu, Z.X. Wang, L.Q. Chen, Phys. Chem. Chem. Phys. 13 (2011) 15127.
[27] Y.B. He, B.H. Li, M. Liu, C. Zhang, W. Lv, C. Yang, J. Li, H.D. Du, B. Zhang, Q.H. Yang, J.K. Kim, F.Y. Kang, Sci. Rep. 2 (2012) 913.
[28] Y.B. He, F. Ning, B.H. Li, Q.S. Song, W. Lv, H.D. Du, D.Y. Zhai, F.Y. Su, Q.H. Yang, F.Y. Kang, J. Power Sources 202 (2012) 253–261.
[29] W. Li, X. Li, M.Z. Chen, Z.W. Xie, J.X. Zhang, S.Q. Dong, M.Z. Qu, Electrochim. Acta 139 (2014) 104.
[30] K.S. Tan, M.V. Reddy, G.V. Subba Rao, B.V.R. Chowdari, J. Power Sources 141 (2005) 129.
[31] M.V. Reddy, G.V. Subba Rao, B.V.R. Chowdari, Electrochim. Acta 50 (2005) 3375.
[32] M.V. Reddy, G.V. Subba Rao, B.V.R. Chowdari, Chem. Rev. 113 (2013) 5364.
[33] Y.K. Sun, J.M. Han, S.T. Myung, S.W. Lee, K. Aminec, Electrochem. Commun. 8 (2006) 821.
[34] K.S. Lee, S.T. Myung, D. Won Kim, Y.K. Sun, J. Power Sources 196 (2011) 6974.
[35] Y.K. Sun, M.J. Lee, C.S. Yoon, J. Hassoun, K. Amine, B. Scrosati, Adv. Mater 24 (2012) 1192.
[36] S.H. Lee, C.S. Yoon, K. Aminec, Y.K. Sun, J. Power Sources 234 (2013) 201.
[37] J.M. Zheng, Z.R. Zhang, X.B. Wu, Z. Zhu, Y. Yang, J. Electrochem. Soc. 155 (2008) 775.
[38] S.J. Shi, J.P. Tu, Y.Y. Tang, Y.Q. Zhang, X.Y. Liu, X.L. Wang, C.D. Gu, J. Power Sources 225 (2013) 338.
[39] J.G. Li, L. Wang, Q. Zhang, X.M. He, J. Power Sources 190 (2009) 149.
[40] S.J. Shi, J.P. Tu, Y.J. Mai, Y.Q. Zhang, Y.Y. Tang, X.L. Wang, Electrochim. Acta 83 (2012) 105.
[41] M.V. Reddy, N. Sharma, S. Adams, R. Prasada Rao, V.K. Peterson, B.V.R. Chowdari, RSC Adv. 5 (2015) 29535.
[42] M.V. Reddy, G.V. Subba Rao, B.V.R. Chowdari, J. Power Sources 195 (2010) 5768–5774.
[43] Y.H. Rho, L.F. Nazar, L. Perry, D. Ryan, J. Electrochem. Soc. 154 (2007) A283.
[44] H. Bryngelsson, M. Stjerndahl, T. Gustafsson, K. Edstrom, J. Power Sources 174 (2007) 970.
[45] M.V. Reddy, B.L.W. Wen, K.P. Loh, B.V.R. Chowdari, ACS Appl. Mater. Interfaces 5 (2013) 7777–7785.
[46] M.V. Reddy, G.V. Subba Rao, B.V.R. Chowdari, J. Mater. Chem. 21 (2011) 10009.